

A Study of the $\lambda 10830$ He I Line Among Red Giants in Messier 13¹

Graeme H. Smith

*University of California Observatories, Lick Observatory, Department of Astronomy &
Astrophysics, UC Santa Cruz, 1156 High St., Santa Cruz, CA 95064, USA*

graeme@ucolick.org

Andrea K. Dupree

Harvard-Smithsonian Center for Astrophysics, Cambridge, MA 02138, USA

dupree@cfa.harvard.edu

Jay Strader

*Department of Physics and Astronomy, Michigan State University, East Lansing, MI
48824, USA*

strader@pa.msu.edu

ABSTRACT

Two properties of Messier 13 are pertinent to the study of mass loss among metal-poor stars and the chemical evolution of globular clusters: (i) an extended blue horizontal branch, which seems to demand mass loss from red giant progenitor stars and possibly an enhanced helium abundance, and (ii) the presence of internal abundance inhomogeneities of elements in the mass range from C to Al. A popular explanation for this second phenomenon is that M13 was self-enriched by intermediate-mass asymptotic giant branch (IM-AGB) stars of a type that may also have been able to instigate helium enrichment. Spectra of the $\lambda 10830$ absorption feature produced by He I have been obtained by using the NIRSPEC spectrometer on the Keck 2 telescope for seven red giants in M13 chosen to have a range in $\lambda 3883$ CN band strengths, oxygen and sodium abundances. Whereas these spectra do reveal the presence of fast winds among some M13 red giants, they provide little support for helium abundance differences of the type that might have been generated by a burst of IM-AGB star activity within the M13 protocluster.

Subject headings: Stars

1. Introduction

Globular clusters of the Milky Way are odd objects. The inhomogeneity of elements in the C-Al mass range within these systems indicates that they have sustained heterogeneous self-enrichment, however elements such as iron and calcium are typically homogeneous among the stars within a given cluster. The abundance inhomogeneities can be conveniently traced by the strength of absorption bands of CN at 3883 Å (e.g., Smith 1987). Many clusters, such as Messier 13, have a sub-population of CN-strong stars that are enhanced in Na and Al but are depleted in C and O relative to a CN-weak sub-population (e.g., Kraft et al. 1997; Sneden et al. 2004; Cohen & Meléndez 2005; Johnson et al. 2005; Smith & Briley 2006).

Following the suggestion of Cottrell & Da Costa (1981) quite a few efforts have been made to interpret the CN-strong stars (which tend to be enriched in the elements N, Na and Al, but depleted in oxygen) as products of inhomogeneous enrichment of a globular cluster in processed ejecta from intermediate-mass asymptotic giant branch (IM-AGB) stars (e.g., Smith & Norris 1982; Denissenkov et al. 1997; Ventura et al. 2001, 2002; Fenner et al. 2004; Bekki 2011), although other sources of element synthesis are arguably also feasible (e.g., Charbonnel 2009). Some clusters harboring chemical inhomogeneities may also show substructures in the color-magnitude diagram, such as multiple subgiant branches or main sequences, that have been interpreted as requiring inhomogeneities of He abundance (e.g., Norris 2004; Piotto et al. 2005; D’Antona et al. 2005; Bragaglia et al. 2010; di Ciscienzo et al. 2010). Within a self-enrichment scenario invoking IM-AGB stars a correlation between He and the CN sub-populations might be possible (e.g., D’Antona et al. 2002) if the enriching stars eject sufficient quantities of helium, the feasibility of which is the subject of some debate (e.g., Karakas et al. 2006; Catelan et al. 2009).

Helium abundances are hard to determine directly for globular clusters, and are often inferred indirectly from the morphology of, or numbers of stars in, different regions of the color-magnitude diagram. Among blue horizontal stars where helium lines are observable in the spectrum, the derived abundance can be subject to uncertainties of interpretation by diffusion effects, with the study of Villanova et al. (2009) being one exception.

In the near infrared there is a He I triplet transition at 10830 Å that can produce an absorption line from the upper chromosphere of late-type stars, both dwarfs and giants. It is a relatively weak feature that has to be observed at high resolution. Dupree et al.

¹The data presented herein were obtained at the W.M. Keck Observatory, which is operated as a scientific partnership among the California Institute of Technology, the University of California and the National Aeronautics and Space Administration. The Observatory was made possible by the generous financial support of the W.M. Keck Foundation.

(1992) were the first to detect this line in the spectrum of a metal-poor field giant: HD 6833 ($[\text{Fe}/\text{H}] = -0.75$; Luck 1991). Previous observations of the He I line among red giants by Zirin (1982) and O’Brien & Lambert (1986) had been limited to Population I giants.

Smith et al. (2004) and Dupree et al. (2009) reported on the use of the NIRSPEC spectrometer on the Keck 2 telescope to survey the $\lambda 10830$ He I line among Population II stars in a variety of evolutionary states: first ascent red giant branch (RGB) stars, red horizontal branch stars, asymptotic giant branch stars, and semi-regular variables. Two objectives of these studies were to canvas the incidence of He I absorption as a function of position in the color-magnitude diagram and to determine line profiles in a search for mass outflows. The spectra show a variety of phenomena. Whereas some giants do not show a He I line at all, the majority do show some absorption. Among giants brighter than the horizontal branch, it is not uncommon for the He I absorption profile to be extended on the blue side indicative of an outflow. Other stars show a more symmetrical He I absorption line. Interestingly, evidence of outflows is detected among a sizable fraction of red horizontal branch stars.

Dupree et al. (1992) modelled the chromospheric He I 10830 Å transition. Because of its large height of formation this line can reveal systematic bulk motions in the atmospheres of a luminous cool star. The He I line is a pure chromospheric feature with no photospheric, circumstellar, or interstellar component, but it is sensitive to bulk gas motions. Excitation of the line is also sensitive to the ultraviolet photon environment. However, models made by Pasquini et al. (2011) and Dupree & Avrett (2013) demonstrate utility as a He abundance indicator for globular cluster giants.

Some empirical results suggest that the $\lambda 10830$ He I line may be informative to the debate over whether He inhomogeneities exist within globular clusters. In the case of ω Centauri, which exhibits a large inhomogeneity in $[\text{Fe}/\text{H}]$, Dupree et al. (2011) used the Phoenix spectrometer on the GEMINI-S telescope to discover a variation in $\lambda 10830$ He I line strength among 12 red giants chosen to occupy a limited region of the color-magnitude diagram. Although the helium transition was not detected in the most metal-poor population ($[\text{Fe}/\text{H}] < -1.8$), it was identified in the majority of stars with $[\text{Fe}/\text{H}] \geq -1.8$. The appearance of helium correlated more closely with increased $[\text{Al}/\text{Fe}]$ and $[\text{Na}/\text{Fe}]$ abundances than with $[\text{Fe}/\text{H}]$. This is analogous to what would be evinced as a CN-He correlation in a more usual bimodal-CN globular cluster.

Dupree & Avrett (2013) constructed semi-empirical chromosphere models of a pair of giants in ω Cen with strong and weak He lines and derived a difference of $\Delta Y \geq 0.17$ in the He mass fraction. They concluded that the $1.083 \mu\text{m}$ He I line can be used to determine a helium abundance for a cool star through the use of semi-empirical model chromospheres

that are adequately constrained by other spectroscopic features such as the Balmer and Ca II K lines. Furthermore, Pasquini et al. (2011) had earlier found that the He I line provided evidence of a He abundance difference between a pair of Na-rich and Na-poor giants in the cluster NGC 2808.

An example of a globular cluster with pronounced carbon and nitrogen abundance inhomogeneities is the system of Messier 13. Extending to extremely blue colors, the horizontal branch of M13 suggests it as a particularly useful test case for He self-enrichment (e.g., Caloi & D’Antona 2005). Central to the present paper is the question of whether CN-strong giants in a particular region of the RGB exhibit systematically stronger He I lines than CN-weak giants. This paper reports upon the He I transition of a sample of CN-strong and CN-weak red giants in M13 that has been observed with the NIRSPEC spectrometer on the Keck 2 telescope.

In our previous NIRSPEC studies of the He I line in metal-poor giants (Smith et al. 2004; Dupree et al. 2009) the objective has mainly been to search for asymmetries in the line profile indicative of mass motions and outflows. By contrast, the emphasis in this paper is on determining whether CN-strong giants in M13 have greater helium line strengths, and so it is the equivalent width that is of primary interest. Previous work on metal-poor field giants of metallicities similar to M13 has returned equivalent widths in the range 0-100 mÅ (Dupree et al. 2009).

2. Observations and Spectra

Spectra were acquired with the NIRSPEC spectrometer (McLean et al. 1998) on the Keck 2 telescope of seven red giants in Messier 13 along with two giants in the cluster Messier 22. The general nature of the observing run was analogous to the NIRSPEC He I programs reported by Smith et al. (2004) and Dupree et al. (2009).

Smith & Briley (2006) published a compendium of CN-strong and CN-weak giants in Messier 13 based on data from the literature. Program stars were selected from their compilation in such a way as to include both CN-strong and CN-weak giants of comparable luminosities. They are listed in Table 1 together with the visual magnitudes and $(B - V)$ colors tabulated by Smith & Briley (2006). The original star identifications are given in Arp (1955) and Sandage (1970). Following Pilachowski et al. (1996) we adopt an apparent distance modulus of $(m - M)_V = 14.33$ for M13, with the corresponding absolute magnitudes M_V for the observed stars being listed in Table 1. Also tabulated are the values of a CN index denoted m_{CN} which quantifies the strength of the $\lambda 3883$ CN band. The values are as

given by Smith & Briley (2006) while the index itself is defined by Suntzeff (1981).

Ancillary abundance information for the M13 stars observed is listed in Table 2. Column (2) gives the value of a CN-excess index δm_{CN} that is defined by Smith & Briley (2006) and is based on making an empirical correction to the m_{CN} index to take account of the sensitivity of the $\lambda 3883$ CN band to stellar temperature and gravity. It is normalized so that giants with the strongest CN bands have $m_{CN} > 1.0$. On the basis of δm_{CN} the seven stars are classified as CN-strong, CN-intermediate, or CN-weak (denoted by an “s”, “i”, and “w” respectively in Tables 1 and 2). Columns 4 and 5 of Table 2 give the values of $[Na/Fe]$ and $[O/Fe]$ that were compiled by Smith & Briley (2006; their Table 1) based in turn on high resolution spectroscopic analyses by Sneden et al. (2004), Pilachowski et al. (1996) and Cohen & Meléndez (2005). In the case of the $[O/Fe]$ abundances all of the measurements in column 5 come from Sneden et al. (2004). Smith & Briley (2006), building on previous work by Sneden et al. (2004) and Kraft et al. (1992, 1993, 1997), showed that the $\lambda 3883$ CN band strength correlates well with the $[Na/Fe]$ abundance in M13, while also anticorrelating with the $[O/Fe]$ abundance, albeit with some scatter. Thus, use of the CN band strength should be a valid way of also picking out stars with different O and Na variations within the cluster.

A more recent study of sodium and oxygen abundances in M13 is that of Johnson & Pilachowski (2012), which includes 5 of the stars in our NIRSPEC program. The $[Na/Fe]$ and $[O/Fe]$ abundances from Johnson & Pilachowski (2012) are listed in columns 6 and 7 of Table 2. On the basis of location within their plot of $[Na/Fe]$ versus $[O/Fe]$, Johnson & Pilachowski (2012) divided the M13 giants into three groups: primordial (P), intermediate (I) and extreme (E), adopting the O/Na classification scheme of Carretta et al. (2009). Despite the large range in CN strengths all of the stars in our program fall into their intermediate I category, which denotes $[Na/Fe] \geq 0.0$ and $[O/Fe] \geq -0.2$. In Appendix A the sodium and oxygen data of Johnson & Pilachowski (2012) are used to further study the relationship between the abundance inhomogeneities of these elements relative to the $\lambda 3883$ CN band strengths of red giant stars in the M13 cluster.

The two stars in Messier 22 for which spectra were obtained (when M13 was out of range of the Keck 2 telescope) are numbered 69 and 87 in ring 1 of the color-magnitude study of Alcaïno (1977), who measured their apparent magnitudes to be $V = 12.64$ and 12.48 respectively. With an apparent distance modulus of $(m - M)_V = 13.74$ for M22 (Monaco et al. 2004), the absolute magnitudes are $M_V = -1.10$ and -1.26 respectively.

Spectra were obtained on the nights of 2012 June 12 and 13 UT. The NIRSPEC spectrometer can record wavelengths in the range $0.95\text{--}5.4 \mu\text{m}$ via various settings in either a high or a low resolution mode. Observations for our program were made with the high-

resolution cross-dispersed echelle mode of NIRSPEC, using the NIRSPEC-1 blocking filter (bandpass 0.95-1.12 μm) to transmit those orders in the vicinity of the $\lambda 10830$ He I line. An echelle/cross-disperser combination of 62.9/34.96 was used to place the order containing the He I line in a suitable location on the detector. A slit of 0.43×12 arc sec was employed. NIRSPEC has an ALADDIN-2 1024×1024 InSb array detector with 27 μm pixels, that was typically used in the MCDS readout mode for the globular cluster stars. The standard pixel scale along the dispersion direction in the high resolution mode is 0.144 arc sec pixel $^{-1}$, and the 0.43 arc sec slit gives a resolving power of $\sim 24,000$. Exposures were made as either AB nod pairs or in an ABBA nod pattern. Integration times at each position within a nod pattern typically ranged from 1200 s to 1800 s. Table 1 lists the total integration time (in seconds) accumulated for each star. The spectrograph slit was oriented along the parallactic angle appropriate to each observation so that atmospheric dispersion of the starlight was along the length of the slit.

Spectra of the hot stars σ Her and 13 Del were obtained to document telluric absorption over the range of airmass (1.0-1.6) at which the cluster stars were observed. These spectra showed that the radial velocities of both M13 (-240 km s $^{-1}$) and M22 (-146 km s $^{-1}$) place the He I $\lambda 10830$ line far from any telluric absorption. Flat field frames were acquired at the beginning and/or end of each night as well as on several occasions during the two nights when the NIRSPEC server and consequently the NIRSPEC configuration had to be reset. Arc spectra of a XeArNe comparison lamp were also obtained at the beginning and/or end of each night.

Reduction of the NIRSPEC images was accomplished by using the REDSPEC software package to produce stellar spectra of the order containing the $\lambda 10830$ He I line. Initial wavelength calibrations were based on the XeArNe lamp spectra, with these solutions being shifted to match the rest frame of each cluster star. (Each spectrum was shifted so as to place a strong absorption line of Si I at the appropriate rest wavelength of 10827 Å). Spectra were normalized using the IRAF² *continuum* task and fitting the stellar continuum with a 5th order cubic spline.

Counts in the spectra in the vicinity of the $\lambda 10830$ He I line range from 2800 ADU per pixel for star IV-19 to 10000 ADU per pixel for star J3. The gain of the detector was 5.7 e $^{-}$ per ADU. In the region of the He I line the pixel scale is 0.156 Å per pixel.

A montage of the M13 spectra is shown in Fig. 1 with the wavelength scale in each panel

²IRAF is written and supported by the National Optical Astronomy Observatories (NOAO) in Tucson, Arizona. NOAO is operated by the Association of Universities for Research in Astronomy (AURA), Inc. under cooperative agreement with the National Science Foundation.

being that of the rest frame of the designated star. Due to the large negative radial velocity of M13 there are no telluric lines of any significance in the wavelength region covered by Fig. 1. Within the NIRSPEC spectra the He I triplet line of the M13 giants typically has the form of a shallow and broad feature. Located about 3 Å to the blue of the He I feature is the strong Si I transition. Six out of the seven M13 giants observed show a He I line absorption profile. However, for star X24 there is emission at the rest wavelength of the He I line which appears to show a P Cygni profile with absorption blueward of 10,828.5 Å.

The pair of giants observed in M22 show very shallow He I absorption and Si I lines having comparable depths to those of the M13 giants. Spectra of these two stars are presented in Fig. 2. The large negative radial velocity of M22 again has a consequence that there are no telluric lines of any significance in the wavelength region covered by Fig. 2.

Measurements of the equivalent width EW of each He I line were attempted in two ways from continuum-normalized spectra. In one approach the equivalent widths were measured with the IRAF task *splot* using an integration of the observed counts over the wavelength extent of the absorption line as judged by eye. The helium line is shallow and broad, and upon doing a direct integration it is difficult to accurately account for the extent to which the blue wing of the He I line may blend into the $\lambda 10827$ Si I line. The direct integration procedure involved marking the two limits of the He I line where the profile reaches the continuum, and then integrating the data between the two points. In order not to include the Si I line in this approach, the limit on the short wavelength side of the He I line was chosen so as not to intrude upon the red side of the Si I. This approach potentially underestimates the equivalent width of the He I line, which visually seems to be quite broad for many of the M13 giants. As a second approach multiple fits using the IRAF *splot* deblending tool were made to the Si I and He I lines assuming that both had Gaussian profiles. The deblending procedure fits two Gaussians simultaneously, one centered on the Si I line, and the other on the He I line. This second approach, which attempts to correct the He line EW for blending with the Si line profile, gave greater He I equivalent widths than the first approach, but with the added uncertainty that the He line may not be Gaussian in shape or symmetrical. As a consequence both sets of He I equivalent widths, denoted EW_1 and EW_2 respectively according to approaches 1 and 2, are listed in Table 1, along with the equivalent width of the Si I line from the Gaussian fit.

A test was done to ascertain how an error in the continuum fitting can transform into an error in the equivalent width. The value of EW_1 for the He I line was remeasured for three stars after adjusting the continuum level slightly and re-integrating over the line. Changes in the measured equivalent widths spanned 7 to 12% from the average equivalent width, and we adopt a value of 10% as a reasonable assessment of the uncertainty in EW_1 due to continuum

placement errors. We note that for some stars the difference between the values of EW_1 and EW_2 exceed this error estimate from the EW_1 measurements. However, as noted above, the short wavelength wing of the helium line may overlap the wing of the Si I feature, so that the measured value of EW_1 is in some cases a lower limit to the actual equivalent width.

The star X24 shows a P Cygni profile with extended emission and a weak absorption component. Consequently this CN-strong giant does not provide a suitable He I comparison with the other six M13 giants observed, and values are not listed for either EW_1 or EW_2 in Table 1.

3. Results

3.1. The $\lambda 10830$ He I Line Equivalent Width

Equivalent widths EW_1 for the He I line are plotted versus the CN index δm_{CN} in Fig. 3 for the Messier 13 giants, with filled circles denoting CN-strong stars and open circles depicting either CN-weak or CN-intermediate giants. Conspicuous by its absence is any indication that the CN-weak giants have weaker He I lines than the CN-strong stars. Not represented in Fig. 3 due to the P Cygni nature of its He I feature is the CN-strong giant X24.

The alternative set of equivalent widths EW_2 is shown versus δm_{CN} in Fig. 4. As with the preceding figure there is no evidence of a correlation between CN band strength and He line equivalent width. Thus despite uncertainties over the appropriate technique for measuring $EW(\text{He I})$ the conclusion of this paper is that of six M13 red giants there is no evidence of a He-CN correlation, i.e., no evidence that the CN-strong giants have systematically stronger He I lines.

Using sodium or oxygen abundances in place of δm_{CN} does not produce any notable trends.³ Plots of EW_1 versus $[\text{Na}/\text{Fe}]$ and $[\text{O}/\text{Fe}]$ from columns 4 and 5 of Table 2 are shown in Figures 5 and 6. There is no indication of either a correlation between He EW_1 and $[\text{Na}/\text{Fe}]$, or an anticorrelation between He EW_1 and $[\text{O}/\text{Fe}]$. Using the $[\text{Na}/\text{Fe}]$ and $[\text{O}/\text{Fe}]$

³There may be a visual impression of an anticorrelation between $EW_{1,2}(\text{He})$ and CN-band strength in Figs. 3 and 4, or between $EW_1(\text{He})$ and $[\text{Na}/\text{Fe}]$ in Fig. 5. We are reluctant to attach any significance to these possibilities. In both Figs. 5 and 7 if the one data point with the largest value of EW_1 was taken away, or the value of EW_1 reduced by $\sim 10\%$, the appearance of an anticorrelation would be greatly diminished. We prefer instead to stress that the data yield no indication of correlations between $EW(\text{He})$ and either CN band strength or Na abundance.

abundances of Johnson & Pilachowski (2012) would lead to fewer stars in each of Figs. 5 and 6 but no difference in the conclusions.

Consequently, among the stars in our NIRSPEC program there is no evidence that those with strong CN bands and enhanced Na, but comparatively low oxygen abundances, have stronger $\lambda 10830$ He I lines than stars of weak CN, low [Na/Fe], and high [O/Fe]. Whatever primordial enrichment process produced the high sodium but reduced oxygen abundances of the CN-strong stars in Table 1, there is no indication that this process was accompanied by enrichment in helium. Whether there may be some helium-enriched stars in Messier 13 that have eluded our modest sample is discussed in Sec 3.4.

3.2. The $\lambda 10830$ He I Line Profile

Visual comparison of the spectra themselves reveal no consistent pattern in He I lines. Six of the stars in Table 1 can be conveniently divided into three CN-strong/CN-weak (or CN-intermediate) pairs (J3/A1, I-12/IV-19, I-18/II-41) on the basis of their position in the color-magnitude diagram (CMD) as shown in Fig. 7. The giants within each of these three pairs have very similar V magnitudes and $B - V$ colors, with each pair being somewhat separated in the CMD. The colors are corrected for a reddening of $E(B - V) = 0.02$ (Harris 1996). The dashed line represents a fiducial locus for the M13 red giant branch taken from Sandage (1970).

Spectra for the stars in each CN-pair are shown superimposed in Fig. 8. In the J3/A1 pair there is little difference in the $\lambda 10830$ feature between the two stars, while in the case of the I-12/IV-19 pair the CN-strong star I-12 exhibits a weaker He feature. Only among the I-18/II-41 pair does the CN-strong star possibly show slightly more absorption at the rest frame wavelength of the He feature. Figure 8 displays in a visual way, independent of equivalent width measurements, our main finding that the spectra provide no indication that the CN-strong stars in our M13 sample have systematically stronger $\lambda 10830$ He I lines than the CN-weak giants.

The $\lambda 10830$ He I line of the seven M13 giants observed shows a range of profiles. It exhibits for some stars an asymmetric profile that extends blueward towards the Si line. As with the previous studies of the He I line among metal-poor red giants by Smith et al. (2004) and Dupree et al. (2009), there is evidence for some stars in the M13 sample of chromospheric outflows that have imposed extended absorption upon the blue wing of the line.

At the wavelength of the $\lambda 10830$ He I line a radial velocity of -50 km s^{-1} corresponds to

a blue shift in the spectrum of 1.8 \AA . In order for the He I line to exhibit blueward absorption extending to the vicinity of the $\lambda 10827 \text{ Si I}$ line it would be necessary for the chromosphere to contain an outflow whose velocity field reaches $\sim 80 \text{ km s}^{-1}$. Short-wavelength absorption in the He I profile that extends to velocities of this order seems to be present for the stars II-41 and IV-19, the P Cygni star X24, and possibly A1 and I-18. These broadened profiles indicate that the He line is being substantially influenced by the velocity fields of the outer chromospheres of M13 red giants, at least those with absolute magnitude brighter than $M_V = -0.3$. It is worth noting that Suntzeff (1981) considers X24 to be a first-ascent red giant branch star; the P Cygni nature of the He I line is not attributable to an AGB star.

If the He I line is to become a potential tool for He abundance determinations in metal-poor red giants of the Galactic halo, it would seem that mass motions in the chromosphere must be incorporated into the models to derive abundance information.

Mészáros et al. (2009) studied the asymmetries of both $H\alpha$ and Ca II K emission line profiles among red giants in M13. In their sample those red giants with evidence of outflows in either emission profile have absolute magnitudes M_V brighter than -1.4 mag . Another sign of outflow is the velocity shifted core of the $H\alpha$ line which is formed higher in the chromosphere than wing emission. In the Mészáros et al. (2009) sample $H\alpha$ core outflow occurs for stars with $\log(L/L_\odot) \geq 2.5$, which for M13 corresponds to stars brighter than $M_V \sim -0.9$. As such the evidence for outflows from the He I line extends to less luminous giants than those traced by the $H\alpha$ and Ca II K line observations.

3.3. Contrasting M13 and ω Centauri

The He I equivalent widths presented here for the M13 giants can be compared with those found by Dupree et al. (2011) for ω Centauri. Of the M13 stars in Table 1 there are several with values of $EW(\text{He})$ less than 40 m\AA , whereas for the detections in ω Cen the typical values are greater than 50 m\AA and extend to $\sim 200 \text{ m\AA}$. Thus Dupree et al. (2011) find some giants in ω Cen with much stronger $\lambda 10830 \text{ He I}$ lines than are present among either the CN-weak or CN-strong giants of M13 listed in Table 1. So not only is there a lack of a CN-He correlation in M13, but the distribution of $\lambda 10830 \text{ EWs}$ is different from that in ω Cen, and more like that of the Population II field stars in Dupree et al. (2009).

Studies of the horizontal branch morphology of M13 suggest that the helium mass fraction may be as high as $Y \sim 0.30$ among some stars (Dalessandro et al. 2013), and 0.02-0.04 higher than for the comparable metallicity cluster M3. Sandquist et al. (2010), on the other hand, find that the R ratio of M13, a measure of the relative numbers of red

giants and horizontal branch stars (Cassisi et al. 2003), is consistent with a helium mass fraction of $Y = 0.25$, with no evidence for a $\Delta Y \sim 0.04$ enhancement above a standard Big Bang level. By contrast, much larger helium contents of $Y \sim 0.4$ (Norris 2004; Piotto et al. 2005; King et al. 2012; Dupree & Avrett 2013) have been invoked or derived for some stars in ω Centauri. Consequently, the current finding that the $\lambda 10830$ He I feature equivalent widths among red giants in M13 do not extend to the larger values found by Dupree et al. (2009) for ω Cen would seem at least qualitatively consistent with expectations based on the morphologies of the color-magnitude diagrams of these two clusters.

3.4. A Direction for Further Work: Are Helium Enhancements Hiding Among the Most Oxygen-Depleted Giants in M13?

The lowest oxygen abundance among the stars in our NIRSPEC sample is somewhat uncertain. On the basis of the O abundances tabulated in column 4 of Table 2 the most oxygen-poor star for which we have a He I spectrum is I-12, the original [O/Fe] measurement of Sneden et al. (2004) being -0.47 dex. If converted to the oxygen abundance scale of Johnson & Pilachowski (2012), the Sneden et al. abundance for star I-12 would be [O/Fe] ~ -0.38 (see Appendix 1). However, Johnson & Pilachowski (2012) derive a much higher oxygen abundance for this star, finding it to be similar in [O/Fe] to J3. There is no [O/Fe] measurement in the literature for I-18, the third CN-strong stars in our NIRSPEC sample.

There are red giants in M13 that are more oxygen-poor than star I-12. Following Johnson & Pilachowski (2012), it remains a possibility that He enhancements in M13 might be confined to those red giants of the lowest oxygen abundance, namely stars in the E category of Johnson & Pilachowski (2012) for which [O/Fe] < -0.2 . The oxygen abundance of star I-12 found by Sneden et al. (2004) does place it in the E category, but not the result of Johnson & Pilachowski (2012). Regardless of this uncertainty as regards I-12, there are nonetheless red giants of M13 in both the studies of Johnson & Pilachowski (2012) and Sneden et al. (2004) that have oxygen abundances of [O/Fe] < -0.4 . It would seem worthwhile extending He I observations to the most oxygen-poor giants known in M13.

Interpreting the behavior of the $\lambda 10830$ He I line among the most oxygen-deficient giants in M13 may hold challenges. The work of Kraft et al. (1993, 1997) indicated that the very lowest [O/Fe] values within M13 tended to be concentrated among the most luminous giants in the cluster, a result which suggested to them that stellar interior mixing on the upper red giant branch has contributed to the great oxygen depletions. The results of Johnson & Pilachowski (2012) seem to support this, as they themselves stress for several reasons:

(i) all known stars with $[O/Fe] < -0.4$ have luminosities of $\log(L/L_{\odot}) > 2.0$, (ii) among the E population of giants in M13 the average $[O/Fe]$ abundance decreases with increasing luminosity, and (iii) among the highest luminosity giants in the E and I categories there are large differences in $[O/Fe]$ but only small differences in $[Na/Fe]$. Smith et al. (2004) found that the most luminous metal-poor red giants in their field and M13 sample often did not exhibit $\lambda 10830$ He I absorption features. It was this finding that lead us to concentrate our newer NIRSPEC observations on stars in M13 that are well removed in absolute magnitude from the tip of the red giant branch, in an effort to enhance the likelihood of detecting the He I line. This selection, however, drove our program away from the upper reaches of the red giant branch in M13 where the most oxygen-deficient giants seemingly prefer to reside.

Thus, one avenue for further $\lambda 10830$ He I observations would be to focus on the faintest very-oxygen-poor giants in M13, in an effort to determine whether He inhomogeneities occur among those cluster stars with the most extreme O-Na-CN combinations. Such red giants, however, with $\log(L/L_{\odot}) > 2.0$, may have had their oxygen abundances diminished below any primordial (pre-red-giant) level by interior deep mixing, i.e., any He enhancements that are found might not be unambiguously attributable to enrichment of M13 by early generations of intermediate-mass or high-mass stars. The current NIRSPEC sample of Table 1 does encompass a substantial range in CN band strengths, O and Na abundances, while avoiding the most oxygen-depleted giants that might be complicated by (non-convective) deep mixing. As such they depict a reasonable subset of the abundance inhomogeneities in M13, and as such they reflect “typical” levels of primordial enrichment in that cluster. For example, Johnson & Pilachowski (2012) found that giants in their I category constitute almost 65% of the stars in M13, while very-oxygen-poor giants with $[O/Fe] < -0.2$ comprise $\sim 22\%$ of the cluster. Thus the indication of our present NIRSPEC spectroscopy is that He enhancements do not appear to be “typical” products of the primordial enrichment of M13. Observations of the most O-poor giants in M13 are needed to determine whether He enhancements might be present among the most extreme stars in that cluster.

3.5. M13 IV-15

Several red giants in M13 were observed in the He I NIRSPEC program of Smith et al. (2004). The stars observed by them were reasonably luminous, and high up on the red giant branch, brighter than those reported upon in this paper. Some of their M13 stars did not show a He I absorption line. One star that did is number IV-15 in the photographic study of Arp (1955). It is a CN-weak star (Smith & Briley 2006) with an apparent magnitude of $V = 12.96$, making it more than 0.4-1.0 mag brighter than the stars in Table 1. The

equivalent widths of the He I line were measured from this earlier spectrum and found to be $EW_1 = 101 \text{ m}\text{\AA}$ and $EW_2 = 123 \text{ m}\text{\AA}$, which place it at the upper bound of the line strengths of the stars in Table 1. As such, IV-15 seemingly provides no evidence for a positive correlation between CN band strength and He line strength. However, Smith & Briley (2006) classify IV-15 as an asymptotic giant branch star with $(B - V) = 1.04$, and as such it does not make for a straightforward comparison with the M13 red giant branch stars in Table 1 due to the different temperature-gravity relations between the red giant and asymptotic giant branches. Johnson & Pilachowski (2012) measured an oxygen abundance for IV-15 of $[\text{O}/\text{Fe}] = +0.10$, so it does not appear to be an example of an oxygen-poor star. Both Johnson & Pilachowski (2012) and Sneden et al. (2004) find a sodium abundance of $[\text{Na}/\text{Fe}] \sim +0.1$ for this star, which is mid-range for the spread observed in M13. Consequently, IV-15 does not appear to be a candidate for an oxygen-poor but CN and He enhanced star of the type that is missing from the sample in Table 1.

3.6. The M22 Pair

Designated as stars I-53 and I-85 in the color-magnitude study of Arp & Melbourne (1959) the giants referred to in Fig. 2 as Alcaino 1069 and 1087 respectively were included in the abundance study of M22 made by Marino et al. (2011). There is a considerable difference in both oxygen and sodium abundances between the stars in this pairing. The more sodium-rich star is Alc 1087 with $[\text{Na}/\text{Fe}] = 0.59$ compared to 0.29 dex for Alc 1069. There is a sodium-oxygen anticorrelation between these giants, with a difference in $[\text{O}/\text{Fe}]$ of 0.38 dex. Alc 1087 with an oxygen abundance of $[\text{O}/\text{Fe}] = -0.03$ is one of the most oxygen-poor stars in the Marino et al. (2011) study, within which the lowest oxygen abundance encountered is $[\text{O}/\text{Fe}] = -0.10$. Marino et al. (2011) and Roederer et al. (2011) found inhomogeneities in *s*-process elements in M22, with Alc 1069 being a member of the *s*-rich subpopulation and Alc 1087 being *s*-poor. There is also an inhomogeneity in iron and calcium within M22 (Norris & Freeman 1983; Lehnert et al 1991; Anthony-Twarog et al. 1995; Da Costa et al. 2009; Marino et al. 2011; Da Costa & Marino 2011), however the difference in $[\text{Fe}/\text{H}]$ between Alc 1069 (-1.74) and Alc 1087 (-1.81) is modest. Comparing the spectra of these two stars in Fig. 2 reveals a slightly stronger He I feature for Alc 1087, the more oxygen deficient of the pairing. There may be a suggestion here of a modest He-O anticorrelation and He-Na correlation. As such, M22 would be worth further investigation as a possible candidate for He inhomogeneities linked to those of the elements oxygen and sodium.

4. Summary

Whereas inhomogeneities in the abundances of certain elements such as nitrogen are commonplace among the red giants of M13, the $\lambda 10830$ He I spectra presented in this paper do not provide compelling evidence for correlated He enhancements in stars with a strong $\lambda 3883$ CN band, which is a surrogate for the nitrogen abundance. Whereas there is considerable evidence in the literature that heterogeneous primordial enrichment of globular clusters contributed to the inhomogeneities in CN, O, and Na in clusters such as M13, there is no evidence from our NIRSPEC observations that these inhomogeneities extend to the element helium, with a caution noted in the following paragraph.

Circumstantial evidence based on the morphology of the horizontal branch in the color-magnitude diagram suggests that any He inhomogeneities in M13 may be more modest than those derived for ω Cen from the He I line by Dupree & Avrett (2013). A caveat to our results is that $\lambda 10830$ spectra have yet to be obtained for the most oxygen-deficient giants in M13. Oxygen abundances of $[\text{O}/\text{Fe}] < -0.2$ were found by Johnson & Pilachowski (2012) among about 22% of the red giants in M13, and it is upon such stars that further spectroscopy of the He I line would be worth concentrating. Perhaps it is among such stars that He abundance enhancements might be encountered, although the potential occurrence of deep interior mixing within such stars could complicate the interpretation of their origin.

Given that a number of the $\lambda 10830$ He I absorption profiles among the M13 red giants show evidence of mass motions in the chromosphere, it could be challenging to detect modest He variations in the cluster via this technique. A detailed matching of the line profile computed for chromospheric models that incorporate mass outflows would seem to be a necessary prerequisite for a measurement of the He abundance via the $\lambda 10830$ line, unless a large enough number of M13 stars can be surveyed so as to obtain a sample in which the line shows no evidence of asymmetric velocity broadening.

Thanks are extended to Dr. Greg Wirth for serving as the support astronomer on the Keck observing run during which the NIRSPEC observations for this paper were acquired. The authors wish to recognize and acknowledge the very significant cultural role and reverence that the summit of Mauna Kea has always had within the indigenous Hawaiian community. We are most fortunate to have the opportunity to conduct observations from this mountain. Thank you to the referee for a useful review of the manuscript. GHS gratefully acknowledges the support of NSF award AST-0908757.

A. The CN, O, Na Inhomogeneities in Messier 13

The abundance data from Johnson & Pilachowski (2012; JP) allow us to revisit the relationships between CN band strength and $[\text{O}/\text{Fe}]$ and $[\text{Na}/\text{Fe}]$ studied earlier for M13 by Sneden et al. (2004; S04) and Smith & Briley (2006; SB). In Fig. 9 the homogenized $[\text{Na}/\text{Fe}]$ abundances tabulated by Smith & Briley (2006) are plotted versus the Johnson & Pilachowski (2012) determinations, while in Fig. 10 the $[\text{O}/\text{Fe}]$ abundance data from Sneden et al. (2004) and Johnson & Pilachowski (2012) are compared. In both figures a straight line depicts equality between the two abundance sets.

There are 29 stars in common to the $[\text{Na}/\text{Fe}]$ measurements of Johnson & Pilachowski (2012) and the tabulation of Smith & Briley (2006). The mean difference is $[\text{Na}/\text{Fe}](\text{JP}) - [\text{Na}/\text{Fe}](\text{SB}) = -0.04$ with a standard deviation of 0.20 dex. Thus it seems as if the two $[\text{Na}/\text{Fe}]$ abundance sets are on the same system. By contrast, as regards the $[\text{O}/\text{Fe}]$ data there are 22 stars in common between JP and S04, with a mean difference of $[\text{O}/\text{Fe}](\text{JP}) - [\text{O}/\text{Fe}](\text{S04}) = 0.085$ and a standard deviation of 0.21 dex. A dashed line has been added to Fig. 10 to illustrate this mean difference.

Just how well the CN band strength of M13 giants traces the Na and O abundance variations can be judged from Figures 11 and 12 in which the δm_{CN} index is plotted versus $[\text{Na}/\text{Fe}]$ and $[\text{O}/\text{Fe}]$ respectively from Johnson & Pilachowski (2012). In accord with previous findings of Kraft et al. (1993, 1997), Sneden et al. (2004) and Smith & Briley (2006) this pair of figures shows that CN band strength correlates with $[\text{Na}/\text{Fe}]$ abundance while anticorrelating with $[\text{O}/\text{Fe}]$. There is scatter in the relationships, for example, at a given CN band strength there may be a range of $\sim \pm 0.2$ dex in $[\text{Na}/\text{Fe}]$ among the CN-weak giants with $\delta m_{\text{CN}} < 0.5$, and a spread of $\sim \pm 0.1$ dex in $[\text{Na}/\text{Fe}]$ among the CN-strongest giants with $\delta m_{\text{CN}} \geq 1.0$. Based on the scatter seen between the independent $[\text{Na}/\text{Fe}]$ datasets in Fig. 11 it is possible that a considerable component of the scatter in $[\text{Na}/\text{Fe}]$ among the CN-strongest giants stems from measurement uncertainties. Among the CN-weakest giants in Fig. 11 there may be intrinsic scatter in $[\text{Na}/\text{Fe}]$ since Johnson & Pilachowski (2012) assess the average measurement error in their $[\text{Na}/\text{Fe}]$ derivations at 0.08 dex.

There are seven stars in Fig. 12 that fall into the Extreme category having the lowest oxygen abundances ($[\text{O}/\text{Fe}] \leq -0.2$). All seven of these stars are CN-strong with $\delta m_{\text{CN}} \geq 0.9$, and six out of seven have $\delta m_{\text{CN}} \geq 1.0$. Nonetheless there is one giant in Fig. 12 that has both strong CN bands and a very high oxygen abundance of $[\text{O}/\text{Fe}] \sim +0.4$, and several CN-strong giants have $[\text{O}/\text{Fe}]$ close to the solar ratio. Thus although there is on average an anticorrelation between CN band strength and oxygen abundance there may be some intrinsic scatter in the cluster of M13. The usual explanation of the trend seen in Fig. 12 is that the material in the CN-strong giants of M13 has been subjected to the O \rightarrow N cycle

of hydrogen burning (e.g., Wallerstein et al. 1987; Brown et al. 1991; Kraft et al. 1992) relative to the material in the CN-weak giants. Johnson & Pilachowski (2012) discussed the alternative scenarios for how this may have come about through a combination of primordial enrichment of the young M13 protocluster plus interior mixing within current-day red giants during the most advanced stages of RGB evolution. Briley et al. (2002, 2004) and Smith & Briley (2006) had previously discussed the evidence for such a dual-origin to the CNO inhomogeneities in Messier 13.

The relationships between CN, [Na/Fe], and [O/Fe] map into an anticorrelation between [Na/Fe] and [O/Fe] within M13 that has been studied and commented upon by Kraft et al. (1992, 1993, 1997), Sneden et al. (2004), Cohen & Meléndez (2005), and Johnson & Pilachowski (2012). A O-Na anticorrelation has been extensively documented among both red giant branch and horizontal branch stars in many other globular clusters of the Milky Way (e.g., Kraft et al. 1995, 1998; Sneden et al. 1992, 1997; Shetrone & Keane 2000; Ivans et al. 1999, 2001; Ramírez & Cohen 2002; Carretta et al. 2006, 2007a,b,c, 2009, 2014; Gratton et al. 2011, 2012, 2013; Yong & Grundahl 2008; Yong et al. 2005, 2014; and references therein).

REFERENCES

- Alcaino, G. 1977, *A&AS*, 29, 383
- Anthony-Twarog, B. J., Twarog, B. A., & Craig, J. 1995, *PASP*, 107, 32
- Arp, H. C. 1955, *AJ*, 60, 316
- Arp, H. C., & Melbourne, W. G. 1959, *AJ*, 64, 28
- Bekki, K. 2011, *MNRAS*, 412, 2241
- Bragaglia, A., Carretta, E., Gratton, R., D’Orazi, V., Cassisi, S., & Lucatello, S. 2010, *A&A*, 519, 60
- Briley, M. M., Cohen, J. G., & Stetson, P. B. 2002, *ApJ*, 579, L17
- Briley, M. M., Cohen, J. G., & Stetson, P. B. 2004, *AJ*, 127, 1579
- Brown, J. A., Wallerstein, G., & Oke, J. B. 1991, *AJ*, 101, 1693
- Caloi, V., & D’Antona, F. 2005, *A&A*, 435, 987
- Carretta, E., Bragaglia, A., Gratton, R. G., Leone, F., Recio-Blanco, A., & Lucatello, S. 2006, *A&A*, 450, 523
- Carretta, E., Bragaglia, A., Gratton, R. G., Lucatello, S., & Momany, Y. 2007a, *A&A*, 464, 927
- Carretta, E., Bragaglia, A., Gratton, R. G., et al. 2007b, *A&A*, 464, 953
- Carretta, E., Bragaglia, A., Gratton, R. G., et al. 2007c, *A&A*, 464, 967
- Carretta, E., Bragaglia, A., Gratton, R. G., et al. 2009, *A&A*, 505, 117
- Carretta, E., Bragaglia, A., Gratton, R. G., et al. 2014, *A&A*, 564, 60
- Cassisi, S., Salaris, M., & Irwin, A. W. 2003, *ApJ*, 588, 862
- Catelan, M., Grundahl, F., Sweigart, A. V., Valcare, A. A. R., & Cortés, C. 2009, *ApJ*, 695, L97
- Charbonnel, C. 2009, in *Star Clusters: Basic Galactic Building Blocks Throughout Time and Space*, Proceedings of the International Astronomical Union, IAU Symposium 266, Cambridge Univ Press, p. 131
- Cohen, J. G., & Meléndez, J. 2005, *AJ*, 129, 303
- Cottrell, P. L., & Da Costa, G. S. 1981, *ApJ*, 245, L79
- Da Costa, G. S., Held, E. V., Saviane, I., & Gullieuszik, M. 2009, *ApJ*, 705, 1481
- Da Costa, G. S., & Marino, A. F. 2011, *PASA*, 28, 28

- D’Antona, F., Bellazzini, M., Caloi, V., Pecci, F. F., Galletti, S., & Rood, R. T. 2005, *ApJ*, 631, 868
- D’Antona, F., Caloi, V., Montalbán, J., Ventura, P., & Gratton, R. 2002, *A&A*, 395, 69
- Dallessandro, E., Salaris, M., Ferraro, F. R., Mucciarelli, A., & Cassisi, S. 2013, *MNRAS*, 430, 459
- Denissenkov, P. A., Weiss, A., & Wagenhuber, J. 1997, *A&A*, 320, 115
- di Criscienzo, M., Ventura, P., D’Antona, F., Milone, A., & Piotto, G. 2010, *MNRAS*, 408, 999
- Dupree, A. K., & Avrett, E. H. 2013, *ApJ*, 773, L28
- Dupree, A. K., Sasselov, D. D., & Lester, J. B. 1992, *ApJ*, 387, L85
- Dupree, A. K., Smith, G. H., & Strader, J. 2009, *AJ*, 138, 1485
- Dupree, A. K., Strader, J., & Smith, G. H. 2011, *ApJ*, 728, 155
- Fenner, Y., Campbell, S., Karakas, A. I., Lattanzio, J. C., & Gibson, B. K. 2004, *MNRAS*, 353, 789
- Gratton, R. G., Lucatello, S., Carretta, E., Bragaglia, A., D’Orazi, V., & Al Momany, Y. 2011, *A&A*, 549, 41
- Gratton, R. G., Lucatello, S., Carretta, E., Bragaglia, A., D’Orazi, V., Al Momany, Y., Sollima, A., Solaris, M., & Cassisi, S. 2012, *A&A*, 549, 41
- Gratton, R. G., Lucatello, S., Sollima, A., et al. 2013, *A&A*, 549, 41
- Harris, W. E. 1996, *AJ*, 112, 1487
- Ivans, I. I., Kraft, R. P., Sneden, C., Smith, G. H., Rich, R. M., & Shetrone, M. 2001, *AJ*, 122, 1438
- Ivans, I. I., Sneden, C., Kraft, R. P., Suntzeff, N. B., Smith, V. V., Langer, G. E., & Fulbright, J. P. 1999, *AJ*, 118, 1273
- Johnson, C. I., Kraft, R. P., Pilachowski, C. A., Sneden, C., Ivans, I. I., & Benman, G. 2005, *PASP*, 117, 1308
- Johnson, C. I., & Pilachowski, C. A. 2012, *ApJ*, 754, L38
- Karakas, A. I., Fenner, Y., Sills, A., Campbell, S. W., & Lattanzio, J. C. 2006, *ApJ*, 652, 1240
- King, I. R., Bedin, L. R., Cassisi, S., Milone, A. P., Bellini, A., Piotto, G., Anderson, J., Pietrinferni, A., & Cordier, D. 2012, *AJ*, 144, 5
- Kraft, R. P., Sneden, C., Langer, G. E., & Prosser, C. F. 1992, *AJ*, 104, 645

- Kraft, R. P., Sneden, C., Langer, G. E., & Shetrone, M. D. 1993, *AJ*, 106, 1490
- Kraft, R. P., Sneden, C., Langer, G. E., Shetrone, M. D., & Bolte, M. 1995, *AJ*, 109, 2586
- Kraft, R. P., Sneden, S., Smith, G. H., Shetrone, M. D., & Fulbright, J. 1998, *AJ*, 115, 1500
- Kraft, R. P., Sneden, S., Smith, G. H., Shetrone, M. D., Langer, G. E., & Pilachowski, C. A. 1997, *AJ*, 113, 279
- Lehnert, M. D., Bell, R. A., & Cohen, J. G. 1991, *ApJ*, 367, 514
- Luck, R. E. 1991, *ApJS*, 75, 579
- Marino, A. F., et al. 2011, *A&A*, 532, A8
- McLean, I. S., et al. 1998, *SPIE*, 3354, 566
- Mészáros, S., Dupree, A. K., & Szalai, T. 2009, *AJ*, 137, 4282
- Monaco, L., Pancino, E., Ferraro, F. R., & Ballazzini, M. 2004, *MNRAS*, 349, 1278
- Norris, J. E. 2004, *ApJ*, 612, L25
- Norris, J., & Freeman, K. C. 1983, *ApJ*, 266, 130
- O’Brien, G., & Lambert, D. 1986, *ApJS*, 62, 899
- Pasquini, L., Mauas, P., Käufl, H. U., & Cacciari, C. 2011, *A&A*, 531, 35
- Pilachowski, C. A., Sneden, C., Kraft, R. P., & Langer, G. E. 1996, *AJ*, 112, 545
- Piotto, G., et al. 2005, *ApJ*, 621, 777
- Ramírez, S. V., & Cohen, J. G. 2002, *AJ*, 123, 3277
- Roederer, I. U., Marino, A. F., & Sneden, C. 2011, *ApJ*, 742, 37
- Sandage, A. 1970, *ApJ*, 162, 841
- Sandquist, E. L., Gordon, M., Levine, D., & Bolte, M. 2010, *AJ*, 139, 2374
- Shetrone, M. D., & Keane, M. J. 2000, *AJ*, 119, 840
- Smith, G. H. 1987, *PASP*, 99, 67
- Smith, G. H. 2007, *Obs*, 127, 301
- Smith, G. H., & Briley, M. M. 2006, *PASP*, 118, 740
- Smith, G. H., Dupree, A. K., & Strader, J. 2004, *PASP*, 116, 819
- Smith, G. H., & Norris, 1982, *ApJ*, 254, 594
- Sneden, C., Kraft, R. P., Guhathakurta, P., Peterson, R. C., & Fulbright, J. P. 2004, *AJ*, 127, 2162
- Sneden, C., Kraft, R. P., Prosser, C. F., & Langer, G. E. 1992, *AJ*, 104, 2121

- Snedden, C., Kraft, Shetrone, M. D., Smith, G. H., Langer, G. E., & Prosserm C. F. 1997, AJ, 114, 1964
- Suntzeff, N. B. 1981, ApJS, 47, 1
- Ventura, P., D’Antona, F., Mazitelli, I., & Gratton 2001, ApJ, 550, L65
- Ventura, P., D’Antona, F., & Mazitelli, I. 2002, A&A, 393, 215
- Villanova, S., Piotto, G., & Gratton, R. G. 2009, A&A, 499, 75
- Wallerstein, G., Leep, E. M., & Oke, J. B. 1987, AJ, 93, 1137
- Yong, D., Alves Brito, A., Da Costas, G. S., et al. 2014, MNRAS, 439, 2638
- Yong, D., & Grundahl, F. 2008, ApJ, 672, L29
- Yong, D., Grundahl, F., Nissen, P. E., Jensen, H. R., & Lambert, D. L. 2005, A&A, 438, 875
- Zirin, H. 1982, ApJ, 260, 655

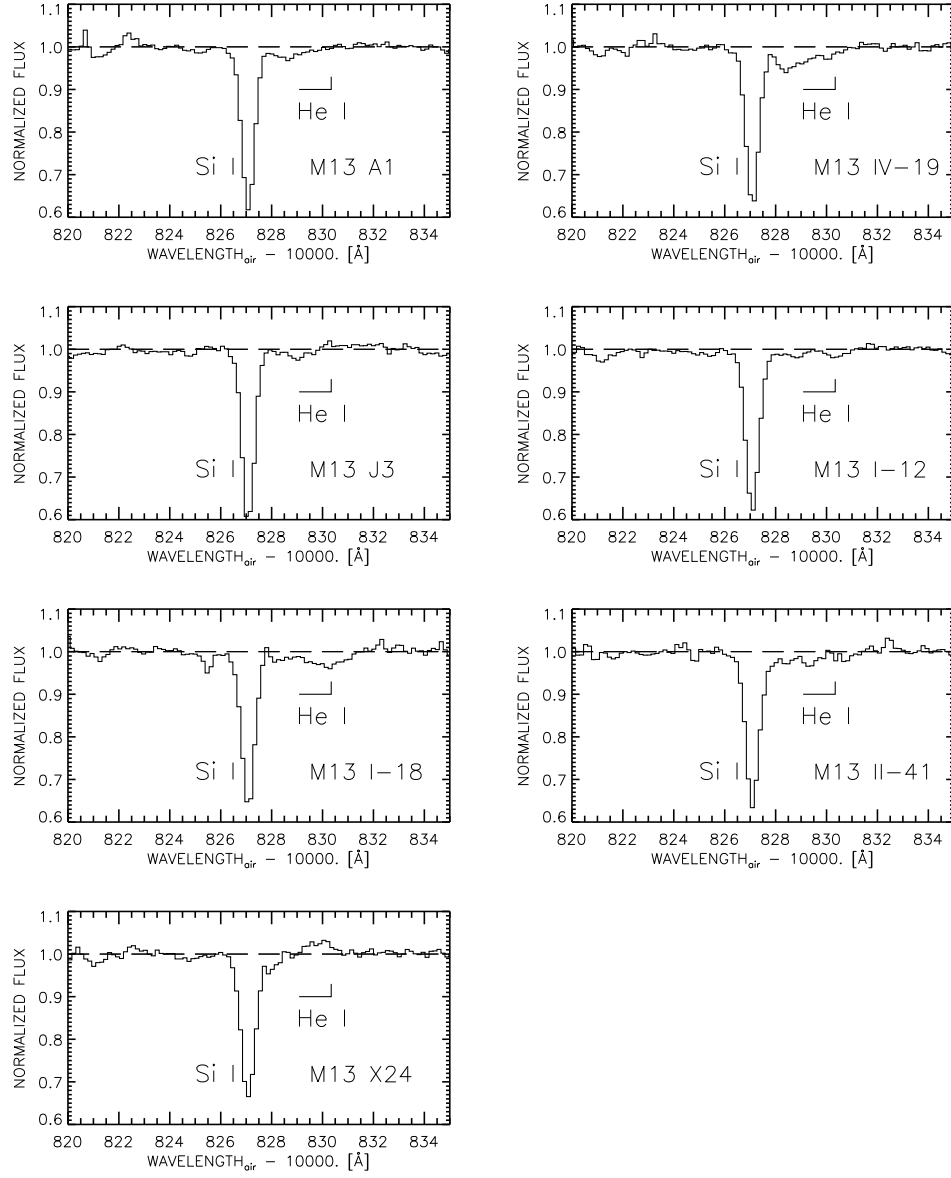


Fig. 1.— Spectra in the vicinity of the $\lambda 10830$ He I feature for seven red giants in the globular cluster Messier 13.

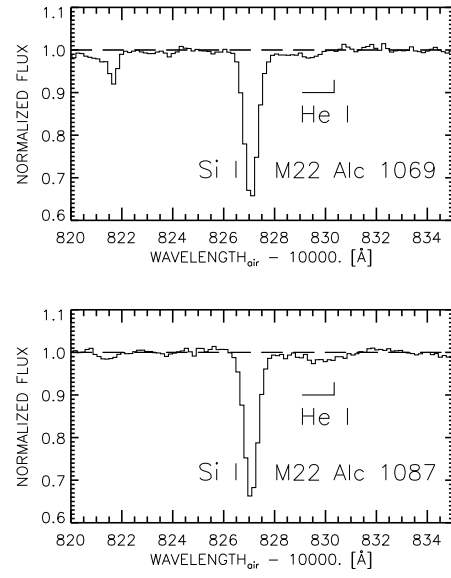


Fig. 2.— Spectra in the vicinity of the $\lambda 10830$ He I feature for two red giants in the globular cluster Messier 22.

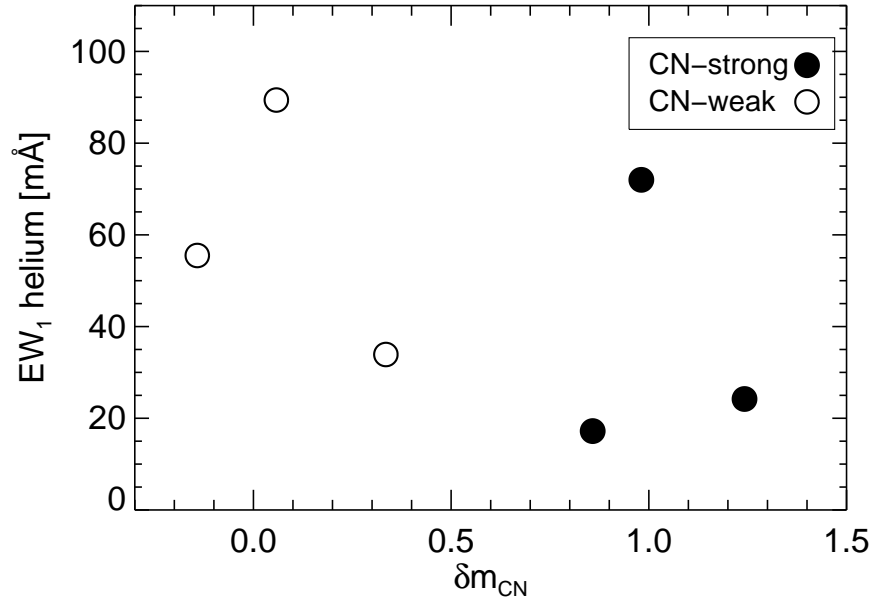


Fig. 3.— The EW_1 measurement of the equivalent width of the He I 10830 Å line versus the CN index δm_{CN} for Messier 13 giants. Filled and open circles denote CN-strong and CN-weak/CN-intermediate giants respectively. Due to its He I line having a P Cygni profile the star X24 is not shown in the figure.

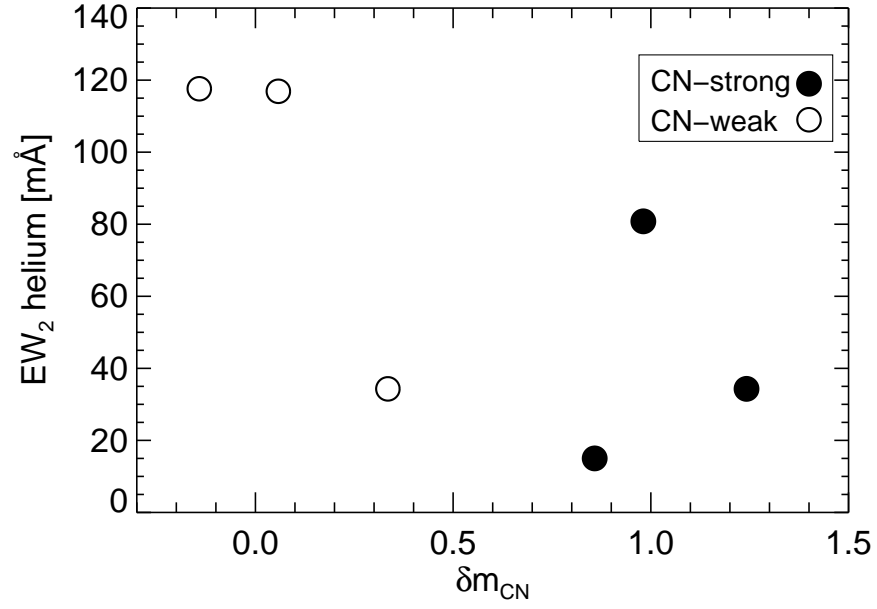


Fig. 4.— The EW_2 measurement (deblended profile) of the He I line equivalent width versus the δm_{CN} CN index for Messier 13 giants. Filled and open circles denote CN-strong and CN-weak/CN-intermediate giants respectively. Star X24 is not shown.

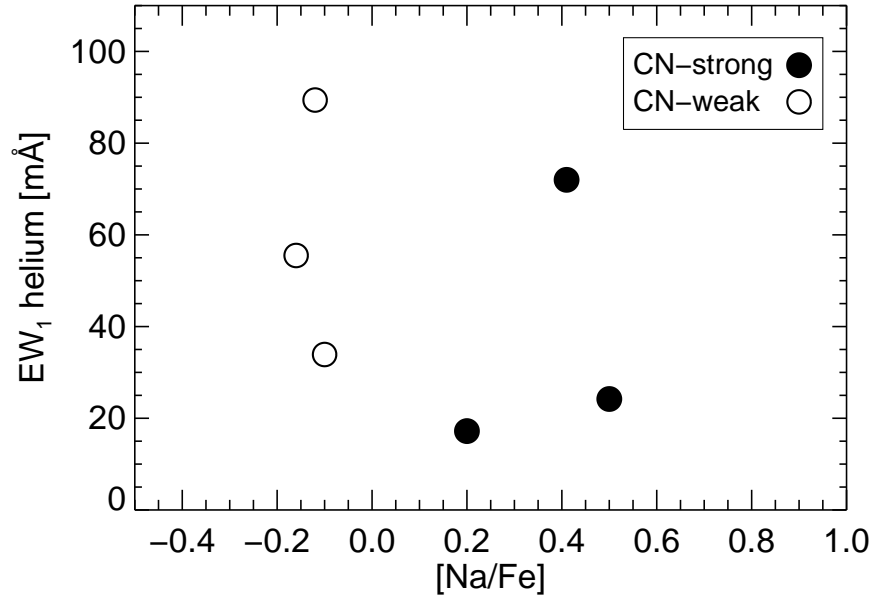


Fig. 5.— The EW_1 measurement of the equivalent width of the He I 10830 Å line versus $[Na/Fe]$ abundance from column 5 of Table 2 for Messier 13 giants. Filled and open circles denote CN-strong and CN-weak/CN-intermediate giants respectively. Star X24 is excluded from the figure on account of exhibiting a P Cygni profile in the He I line.

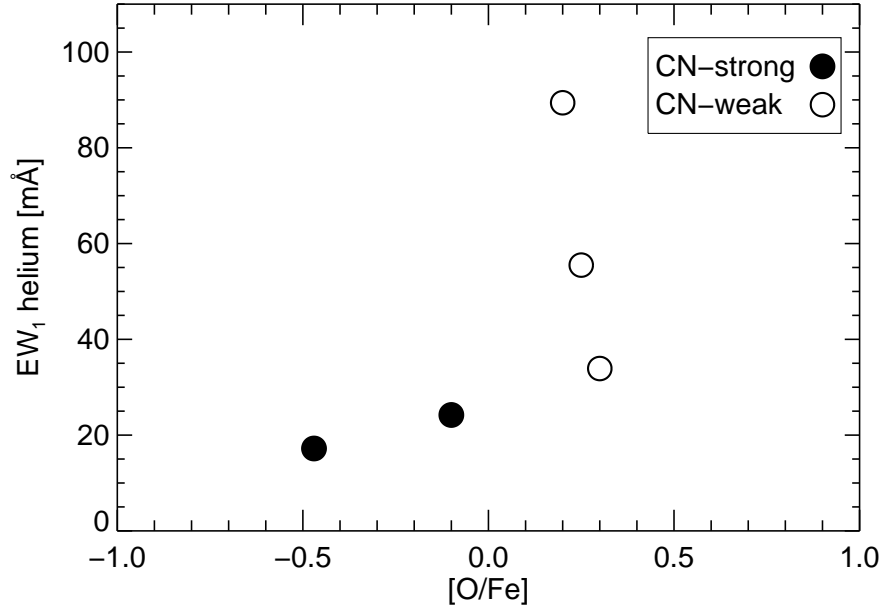


Fig. 6.— The equivalent width EW_1 of the He I 10830 Å line versus [O/Fe] abundance from column 4 of Table 2 for M13 giants. Filled and open circles denote CN-strong and CN-weak/CN-intermediate giants respectively. Star X24 is again omitted from the plot due to a P Cygni profile in the He I line.

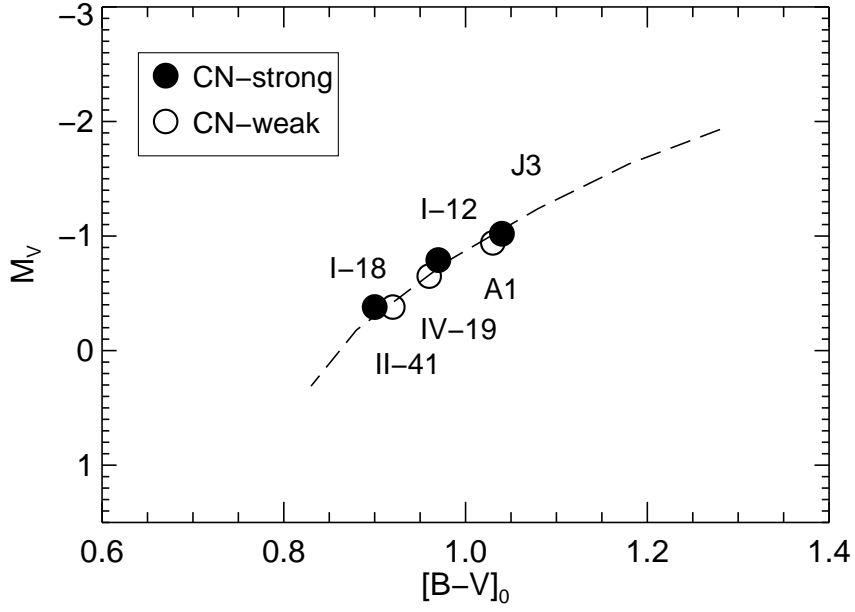


Fig. 7.— The color-magnitude diagram of three pairs of Messier 13 giants with NIRSPEC spectroscopy. Filled and open circles denote CN-strong and CN-weak/CN-intermediate giants respectively. Star X24 is not shown. Each point is labelled with the designation of each star, while the dashed line is based on the fiducial red giant branch of Sandage (1970).

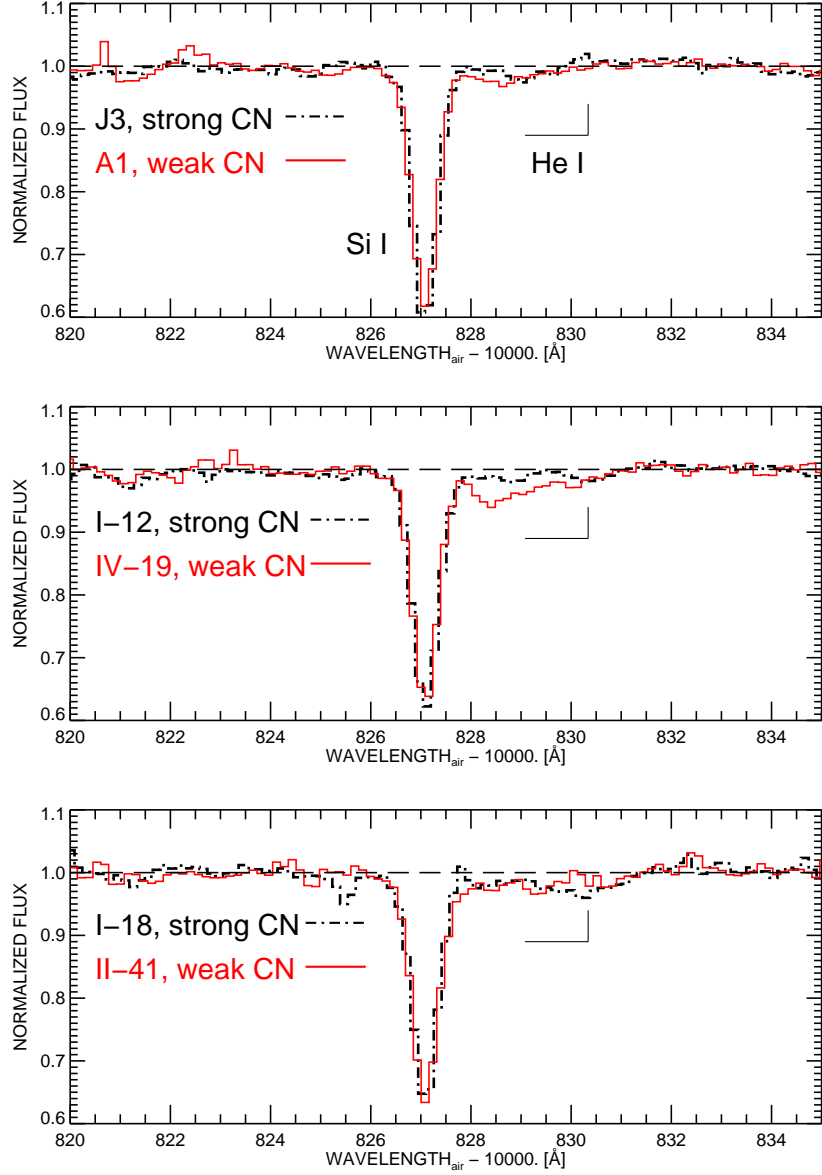


Fig. 8.— Spectra covering the wavelength range $\lambda\lambda 10820\text{--}10835$ Å for three pairs of giants in M13. The horizontal axis plots the rest frame wavelength minus 10000 Å. The stars in each pair have similar absolute visual magnitudes and $B - V$ colors but differ in $\lambda 3883$ CN band strength. In each panel the spectrum of the CN-strongest giant is shown as a black (broken) line, while the spectrum of the CN-weaker giant is depicted with a red (solid) line. The location of the $\lambda 10830$ He I feature is indicated by the horizontal line.

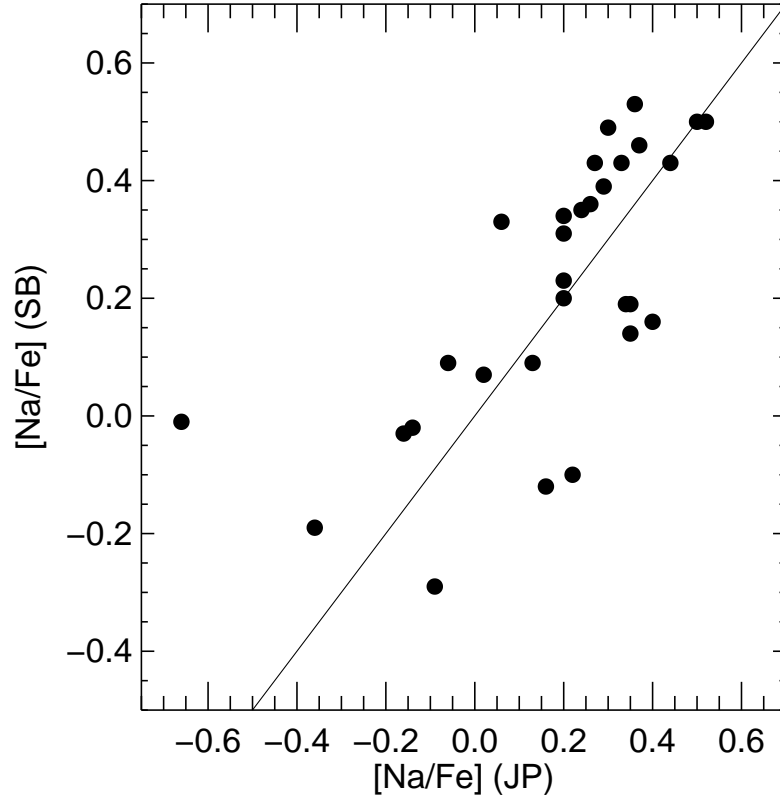


Fig. 9.— The homogenized [Na/Fe] abundances from Smith & Briley (2006) versus Johnson & Pilachowski (2012) determinations. A straight line depicts equality between the two abundance sets.

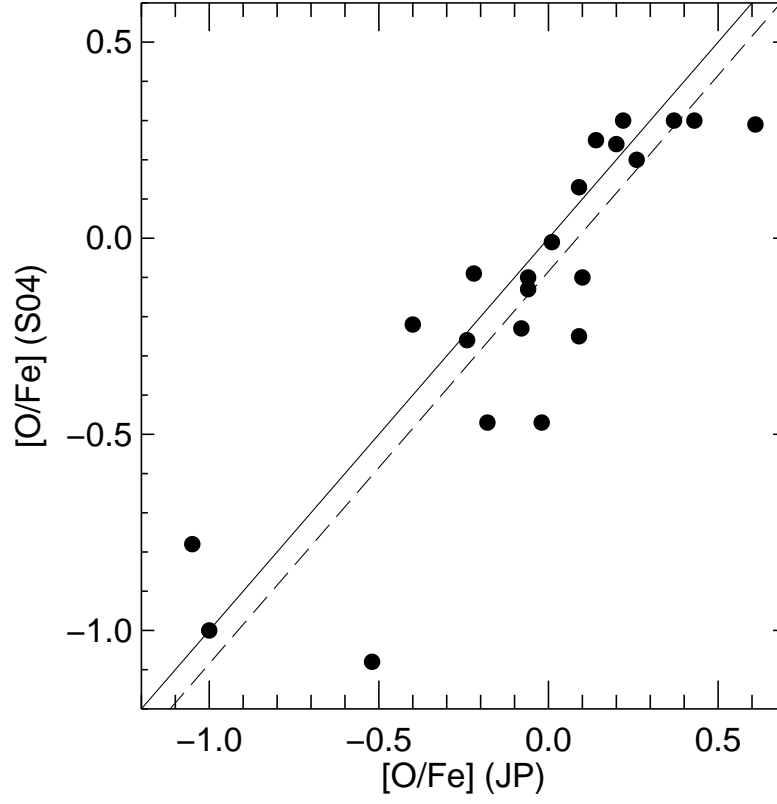


Fig. 10.— Oxygen abundance data from Sneden et al. (2004) versus measurements from Johnson & Pilachowski (2012). A straight line depicts equality between the two abundance sets, while the dashed line is offset by 0.085 dex.

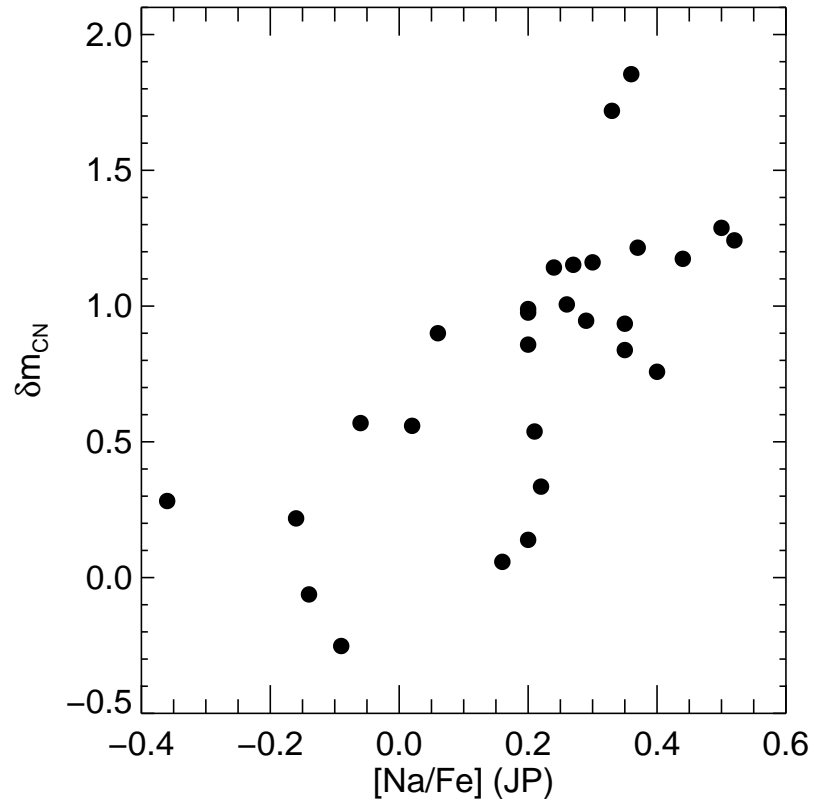


Fig. 11.— The δm_{CN} CN-band index versus $[Na/Fe]$ measurements from Johnson & Pilachowski (2012) for red giants in M13. There is a notable correlation.

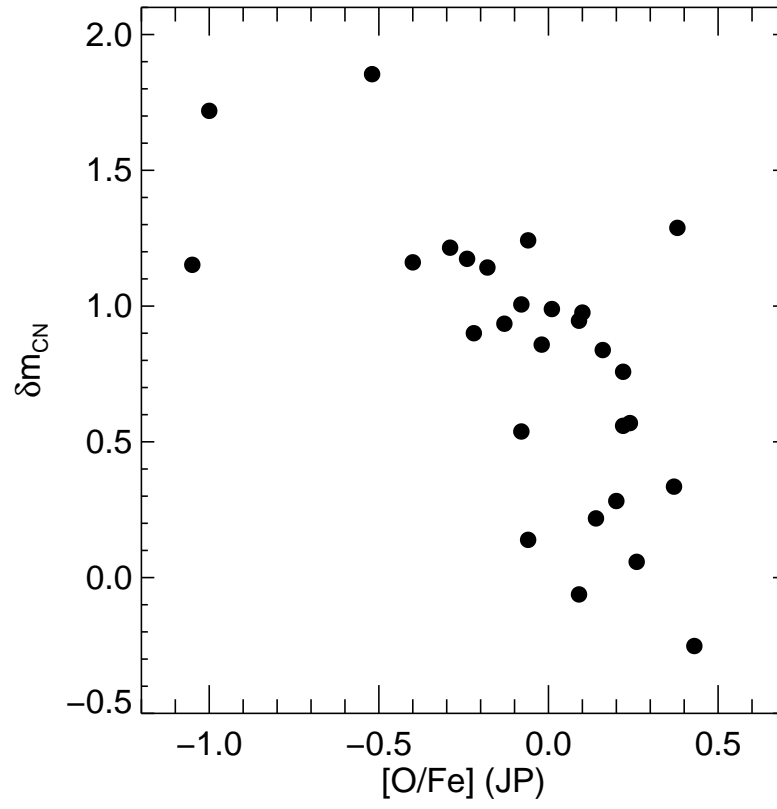


Fig. 12.— The δm_{CN} CN-band index versus $[O/Fe]$ abundance from Johnson & Pilachowski (2012) for red giants in M13. There is a notable anticorrelation.

Table 1. Observational Data for Red Giants in Messier 13

Star	Exp (s)	V	M_V	$B - V$	m_{CN}	CN class	EW_1 (He I) (mÅ)	EW_2 (He I) (mÅ)	EW (Si I) (mÅ)
I-12	4800	13.54	−0.79	0.99	0.342	s	17.2	15.0	244.8
I-18	6000	13.95	−0.38	0.92	0.333	s	72.0	80.8	236.8
II-41	6000	13.95	−0.38	0.94	0.041	w	55.5	117.6	224.1
IV-19	4800	13.68	−0.65	0.98	0.120	w	89.4	116.9	218.0
A1	3600	13.39	−0.94	1.05	0.221	i	33.9	34.3	235.8
J3	3600	13.31	−1.02	1.06	0.465	s	24.2	34.3	251.5
X24	6000	13.75	−0.58	0.95	0.295	s	PCyg	PCyg	233.6

Table 2. Abundance Data for Program Stars in Messier 13

Star	δm_{CN}	CN class	[O/Fe] SB ^a	[Na/Fe] Sn04,SB ^b	[O/Fe] JP ^c	[Na/Fe] JP
1	2	3	4	5	6	7
I-12	0.858	s	−0.47	0.20	−0.02	0.20
I-18	0.981	s	0.41
II-41	−0.142	w	0.25	−0.16
IV-19	0.058	w	0.20	−0.12	0.26	0.16
A1	0.335	i	0.30	−0.10	0.37	0.22
J3	1.242	s	−0.10	0.50	−0.06	0.52
X24	0.758	s	0.16	0.22	0.40

^aSmith & Briley (2006).

^bAbundances from Sneden et al. 2004 as tabulated in Smith & Briley (2006).

^cJohnson & Pilachowski (2012).